Chemistry of Metals and Alloys

Chem. Met. Alloys 19 (2026) 17-26
ISSN 1998-8079 (print), ISSN 1998-8087 (online)
Ivan Franko National University of Lviv
https://publications.lnu.edu.ua/chemetal

Sc–Ru phase diagram revised by diffusion couple and classical approaches: discovery and crystal structure of the Sc_3Ru_2 compound

Serena DE NEGRI[1]*, Pavlo SOLOKHA[1]

[1] *Dipartimento di Chimica e Chimica Industriale, Università degli Studi di Genova, via Dodecaneso 31, 16146 Genova, Italy*
* *Corresponding author. Tel.: +39-010-3356159; e-mail: serena.denegri@unige.it*

Received April 28, 2026; accepted June 25, 2026, available online September 8, 2026
https://doi.org/10.30970/cma19.0461

The Sc–Ru phase diagram was partially re-investigated at high temperatures by combining diffusion-couple experiments with the preparation and characterization of selected key alloys. Phase compositions and crystal structures were investigated by SEM/EDXS and by single-crystal and powder XRD. In the diffusion couples continuous interdiffusion zones containing the intermediate compounds $ScRu_2$, ScRu, Sc_3Ru_2, Sc_2Ru, $Sc_{11}Ru_4$, $Sc_{57}Ru_{13}$ were formed, with no appreciable terminal solid solubilities. All the observed binary compounds are essentially stoichiometric. The previously reported Sc_5Ru_3 phase was not detected in any of the diffusion couples or key alloys, whereas $Sc_{44}Ru_7$ formed only after thermal cycling of a Sc-rich alloy up to 1450°C. A previously unreported compound of Sc_3Ru_2 stoichiometry was identified and its crystal structure determined; it crystallizes in the tetragonal Al_3Os_2 type (space group *I*4/*mmm*, Pearson symbol *tI*10), with lattice parameters *a* = 3.2432(3) Å and *c* = 17.337(3) Å. This investigation demonstrates the efficiency of diffusion couples, complemented by targeted alloy synthesis, for resolving inconsistencies between experimental phase diagrams and first-principles predictions.

Diffusion couple / Intermetallic compound / Crystal structure / Phase diagram

Introduction

The knowledge of phase diagrams is an essential pre-requisite for the design, preparation and characterization of new materials, especially in the field of intermetallics. Nowadays the classical experimental approach consisting of synthesis and characterization of many samples is more and more supported by first-principles energy calculations, allowing managing a huge volume of data on composition/structure/properties. For example, the stability of an impressive number of new phases in numerous binary systems was predicted by Curtarolo *et al.* [1,2], generating structural models based on known prototypes and further screening them applying the formation energy criterion. The main drawbacks of this approach are the impossibility to generate and test new structures/homogeneity ranges and the temperature limits (calculations refer to 0 K condition, experimentally unachievable). Therefore, synergy between experiments and calculations is always necessary to obtain the best results, optimizing time, cost and efforts.

The Sc–*T* systems (*T* = transition element) represent a good playground for this idea [3]; as an example, the Sc–Ru convex hull as reported on the AFLOW (Automatic FLOW for materials discovery) site [4] is shown in Fig. 1. In general, there is good agreement with experimental data [5], but some discrepancies can be pointed out:

1) Sc_5Ru_3, reported in the phase diagram, is unstable at absolute zero.
2) The crystal structure suggested for the ground state of Sc_2Ru (*tI*6-Mo_2Si) differs from that reported in [5,6] (*hP*96-Ti_2Ni), and also from that later established by us (*hP*45-Sc_2Ru) [3]. The latter represents a new prototype, and its existence is certain, at least at high temperatures.
3) $Sc_{57}Ru_{13}$, reported in the phase diagram, is slightly unstable at absolute zero.

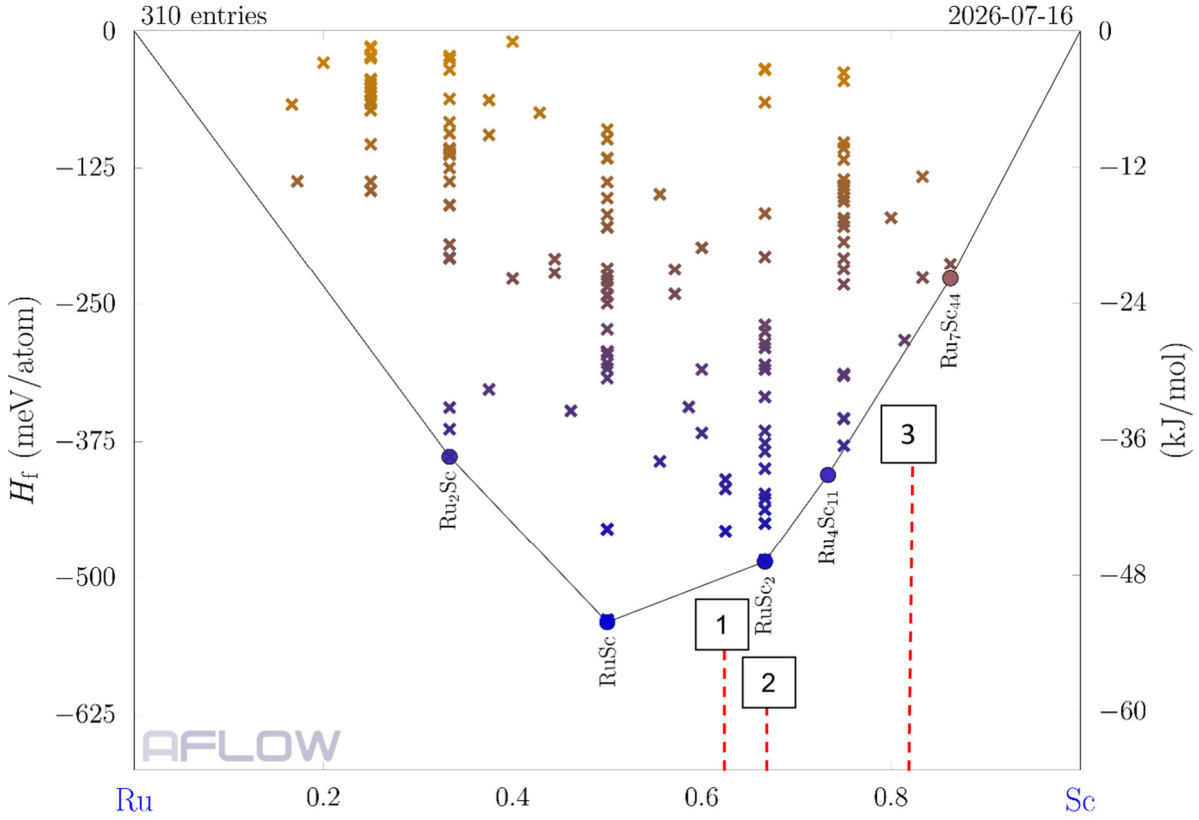


Fig. 1 Sc–Ru convex-hull taken from AFLOW [4]. Red dashed lines highlight discrepancies between experimental and high-throughput data discussed in the text.

Considering these points, the Sc–Ru phase diagram was experimentally checked between 850 and 1000°C joining the classical approach with an alternative one consisting of the preparation and characterization of diffusion couples [7]. This method, not new but strongly underestimated, relies on solid-state diffusion and makes it possible to overcome difficulties and problems arising from classical synthesis from the melt, simultaneously reducing the number of samples and saving time and money.

Experimental details

Sample preparation

Metallic scandium and ruthenium (with nominal purities > 99.9 mass%) were used as starting materials to prepare diffusion couples (DC) and key alloys.

For the DC preparation it was necessary to have end-members in the form of disks. For this purpose, small pieces of Sc sponge were arc-melted together to obtain a spherical ingot, which was incorporated in a polyphenolic thermosetting resin and then cut into 2-mm thick disks (Ø 1.5 cm). A Ru ingot was directly incorporated into the polyphenolic resin and cut into 2-mm thick disks (Ø 1 cm) using a miter saw.

The metal disks, re-embedded in the thermosetting resin, were polished to obtain mirror-like surfaces, necessary for uniform diffusion. Then the mirror-like disk surfaces were put in contact; the samples were wrapped in tantalum foil and pressed inside a threaded steel tube between two steel screws tightened by applying a pressure of 2 bar with a torque wrench. The tube containing the DC was put into a quartz tube sealed under an Ar atmosphere and placed in a resistance furnace for the thermal treatment. After annealing, the quartz tube was quenched in cold water and broken to retrieve the steel tube and extract the couple. Two DCs were prepared: DC_1 (1000°C for 7 days) and DC_2 (850°C for 13 days).

Several Sc–Ru key alloys in the 50-100 at.% Sc compositional range were also produced and characterized: small chunks of the components were weighed in the stoichiometric ratio to obtain the desired composition and arc-melted several times for better homogeneity. For annealing, the samples were put in tantalum crucibles, then in a quartz tube sealed under an Ar atmosphere and finally placed in a resistance furnace at 1000°C for 7 days. One sample was instead submitted to three heating/cooling cycles from room temperature to 1450°C inside a LABSYS EVO device (SETARAM Instrumentation, Caluire, France) equipped with type S (Pt-PtRh 10%) thermocouples.

SEM/EDXS characterization

For microscopic examination, each DC was carefully extracted, pressed in a steel spring and incorporated in epoxy resin. It was then rubbed with sandpaper to expose the cross section of the inner part of the couple for the analysis of the interdiffusion layer. For the key alloys, instead, some pieces of each alloy were directly embedded in the epoxy resin.

All the specimens were rubbed with SiC sandpaper of increasing grit (400, 600, 800, 1000, and 1200 grit), polished with diamond pastes (6, 3, 1, and 0.25 µm), and covered with aluminum foil tape to make them conductive. The microstructure and phase composition were analyzed using a scanning electron microscope (SEM) Zeiss Evo 40 equipped with an Energy-Dispersive X-ray (EDX) Spectroscope Oxford Instruments INCA X-ACT operated by INCA Energy software (Oxford Instruments, Analytical Ltd., Bucks, U.K.). Calibration for the elemental analysis was performed using a cobalt standard.

XRD characterization

The key alloys were characterized by X-ray diffraction, both on single crystals and powders. Single crystals of the already known Sc–Ru phases were extracted from various samples and their crystal structures checked on an Oxford Diffraction Xcalibur Single-Crystal X-ray Diffractometer. The data collection strategy, reduction and integration of the data sets were performed with CrysAlisPRO [8]; the crystal structures were solved with Jana2006 [9].

A metallic silvery, irregularly-shaped crystal of Sc_3Ru_2 was selected from a mechanically crushed alloy under a light microscope and mounted on the goniometer on the tip of a glass fiber. X-ray diffraction data was collected on a three-circle Bruker D8 QUEST diffractometer equipped with a PHOTON III 14 photon counting detector. Graphite-monochromatized Mo *K*α radiation was used. The data collection strategy, applied using the APEX6 software [10], consisted of three ω-scans and two ϕ-scans and covered the reciprocal space up to a maximum θ of about 36° (resolution of *ca.* 0.6 Å) with an exposure of 20 s per frame. A Multi-Scan absorption correction using SADABS 2016/2 was applied [11]. The structure was solved by Intrinsic Phasing methods and refined by full-matrix least-squares methods against F^2 using SHELXL-2019/2 [12,13]. Crystallographic data for Sc_3Ru_2 have been deposited with the Cambridge Crystallographic Data Centre [14], with deposition number 2583792.

Powder X-ray diffraction was used to confirm the crystal structures of the phases in the key alloys and calculate their lattice parameters: a Philips X'Pert MPD Bragg-Brentano diffractometer was used for this purpose (Cu *K*α radiation, continuous scanning mode). PowderCell [15] and CrystalDiffract [16] software was used for indexation; precise lattice parameters were calculated by a least-squares routine.

Results and discussion

Results from the diffusion couples (DC) characterization are shown in Fig. 2 and compared with literature data on phase equilibria.

Both DCs showed quite thick interdiffusion regions of ~200 µm for DC 1 (1000°C) and ~100 µm for DC 2 (850°C), in agreement with Arrhenius' law describing the dependence of the diffusion kinetics on temperature. In both cases prominent cracks were observed (see Fig. 3), which originate from the Kirkendall effect, consisting of accumulation of voids due to a microscopic vacancy diffusion mechanism. In agreement with theory, cracks were observed on the Sc side, since this end-member has the lower melting point and is therefore the faster-diffusing species.

The analysis of both DCs shows reproducible compositions suggesting the following phases (see Fig. 3): Ru, $ScRu_2$, ScRu, $Sc_{60}Ru_{40}$ (not previously reported), Sc_2Ru, $Sc_{11}Ru_4$, $Sc_{57}Ru_{13}$, and Sc. The end-members don't show any significant mutual solubility. It should be stressed that bands with compositions corresponding to the Sc_5Ru_3 and $Sc_{44}Ru_7$ compounds were not observed, confirming the need for experimental revision. The EDXS analyses suggest that all the compounds are stoichiometric, as it is also evident from the concentration profile at 850°C shown in Fig. 4, where the segments corresponding to the different compounds are flat; however, in some cases ($ScRu_2$, ScRu) the layers are very thin and it was not possible to measure many points along them. As a general trend, the layer thickness increases from Ru to Sc, with $Sc_{11}Ru_4$ forming a very broad band (~60 µm at 850°C, representing about half of the entire interdiffusion region).

Considering the results of the DC characterization, the 50-100 at.% Sc region was further checked by studying six key alloys (global compositions are shown in Fig. 2 and the results of their characterization are presented in Table 1, Fig. 5, and Fig. 6). Since the DC results are qualitatively the same, the annealing temperature 1000°C was chosen for the key alloys to approach equilibrium conditions more quickly: in fact, the as-cast alloys frequently contained more than two phases, whereas the annealed ones were generally in equilibrium.

The results obtained on the key alloys confirm many points already observed on the DCs:

- all the binaries are stoichiometric, as deduced both from the measured compositions and the lattice parameters;
- the Sc_5Ru_3 compound was never detected, in agreement with the convex hull (Fig. 1);
- the existence of the $Sc_{60}Ru_{40}$ phase was confirmed, and its crystal structure was solved by single-crystal X-ray diffraction, giving the formula Sc_3Ru_2 (see below).

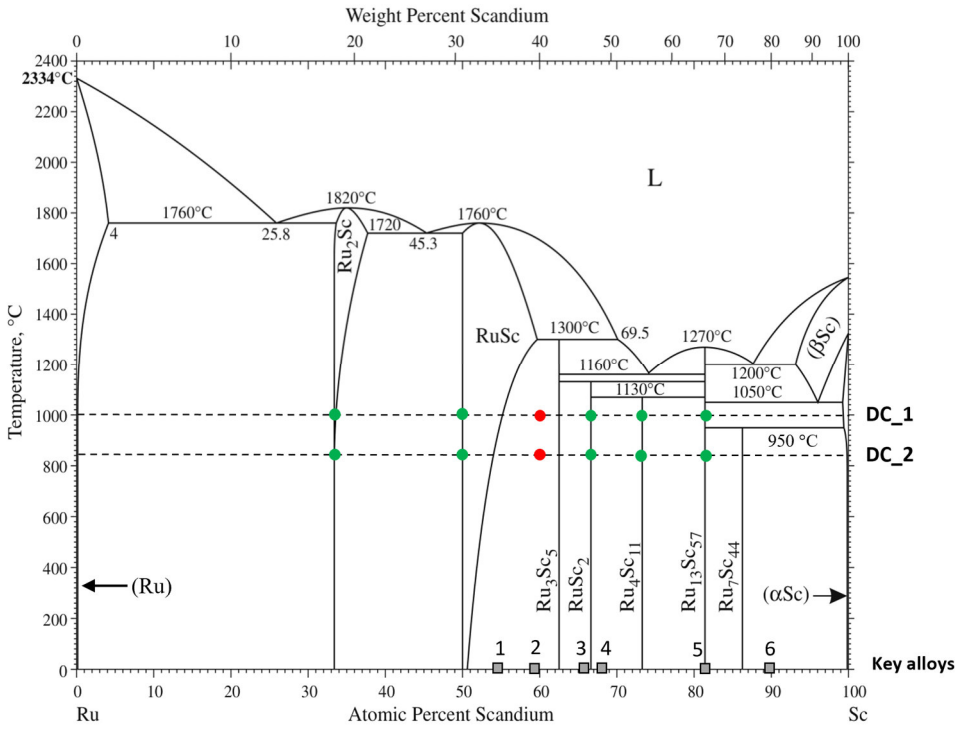
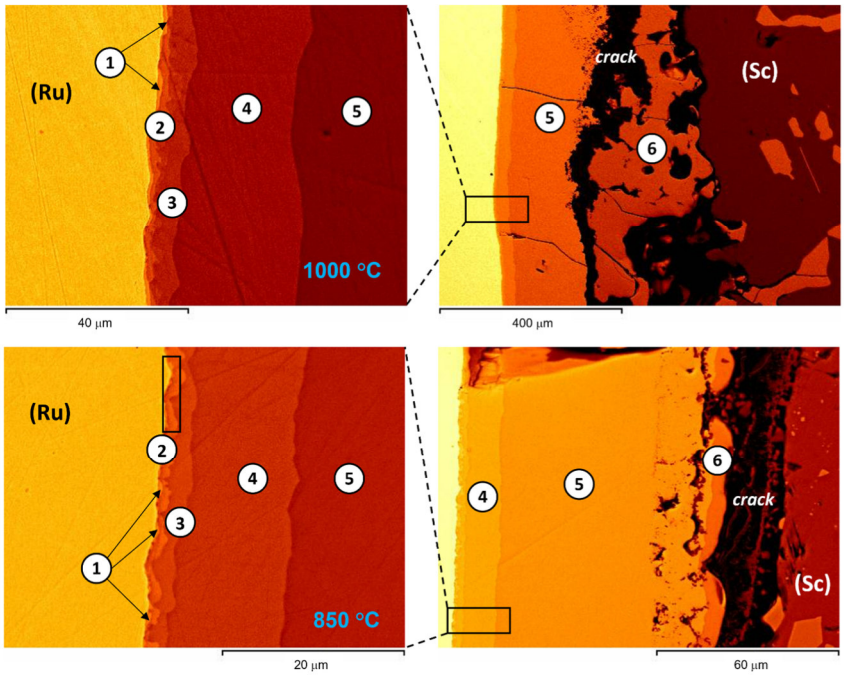


Fig. 2 Sc–Ru phase diagram adapted from [5]: horizontal dashed lines represent the temperatures of the diffusion couples (green circles indicate the compounds confirmed in this work; red circles indicate the new Sc_3Ru_2 phase); grey squares represent the compositions of key alloys).



Band	at.% Sc	Phase
1	34.8	$ScRu_2$
2	51.2	ScRu
3	60.1	Sc_3Ru_2
4	67.1	Sc_2Ru
5	73.5	$Sc_{11}Ru_4$
6	83.0	$Sc_{57}Ru_{13}$

Band	at.% Sc	Phase
1	32.0	$ScRu_2$
2	49.5	ScRu
3	59.0	Sc_3Ru_2
4	65.6	Sc_2Ru
5	72.8	$Sc_{11}Ru_4$
6	83.0	$Sc_{57}Ru_{13}$

Fig. 3 SEM images (BSE mode) of the studied diffusion couples. Enlarged regions are shown on the left. The average value of the composition from EDXS and the phase corresponding to each band are listed on the right.

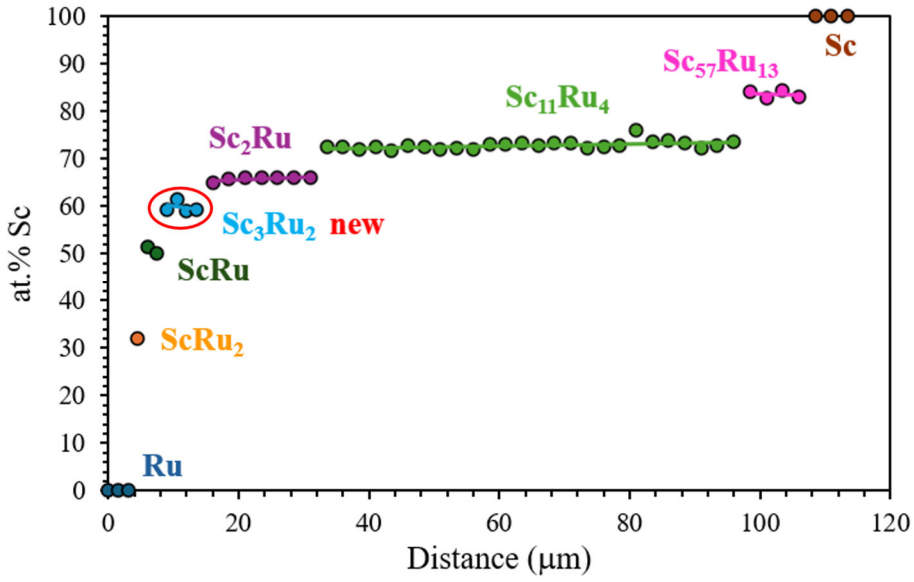


Fig. 4 Sc–Ru concentration profile at 850°C.

Table 1 Results of the SEM/EDXS and XRD characterization of the Sc–Ru key alloys.

Code at.% Sc	Thermal treatment	Phase	Phase comp. (at.% Sc)	Pearson symbol/ prototype	Lattice parameters (Å)		
					a	*b*	*c*
N. 1 54.6	annealed at 1000°C/7d	ScRu[a] Sc_3Ru_2 Sc_2Ru	50.8 59.3 65.5	*cP*2-CsCl *tI*10-Al_3Os_2 *hP*45-Sc_2Ru	3.2185(3) 3.2435(3) 9.3568(5)	– – –	– 17.349(4) 11.2830(7)
N. 2 59.1	as cast	ScRu Sc_3Ru_2 Sc_2Ru $Sc_{11}Ru_4$	51.0 59.1 65.9 72.4	*cP*2-CsCl *tI*10-Al_3Os_2 *hP*45-Sc_2Ru *cF*120-$Zr_{11}Os_4$	3.2201(4) 3.2428(2) 9.3578(4)	– – –	 17.342(3) 11.2834(6)
	annealed at 1000°C/7d	Sc_3Ru_2[a]	59.1	*tI*10-Al_3Os_2	3.2432(3)	–	17.337(3)
N. 3 65.8	annealed at 1000°C/7d	Sc_2Ru	65.9	*hP*45-Sc_2Ru	9.3648(2)	–	11.2942(3)
N. 4 68.0	as cast	Sc_3Ru_2 Sc_2Ru $Sc_{11}Ru_4$	59.7 66.0 72.1	*tI*10-Al_3Os_2 *hP*45-Sc_2Ru *cF*120-$Zr_{11}Os_4$	 9.3600(3) 13.3539(6)	 – –	 11.2875(5) –
	annealed at 1000°C/7d	Sc_2Ru[a] $Sc_{11}Ru_4$[a]	66.0 72.4	*hP*45-Sc_2Ru *cF*120-$Zr_{11}Os_4$	9.3596(6) 13.3582(5)	– –	11.292(1) –
N. 5 81.2	annealed at 1000°C/14d	$Sc_{11}Ru_4$ $Sc_{57}Ru_{13}$[a]	72.8 81.3	*cF*120-$Zr_{11}Os_4$ *cP*140-$Sc_{57}Rh_{13}$	 14.4102(3)	 –	 –
N. 6 89.6	as cast	$Sc_{57}Ru_{13}$ Sc	82.0 100	*cP*140-$Sc_{57}Rh_{13}$ *hP*2-Mg	14.420(2) 3.3104(7)	– –	– 5.273(2)
	after DTA[b]	$Sc_{57}Ru_{13}$ $Sc_{44}Ru_7$[a] Sc	80.7 86.2 100	*cP*140-$Sc_{57}Rh_{13}$ *cF*408-$Mg_{44}Rh_7$ *hP*2-Mg	14.3971(3) 20.7758(3)	– –	– –

[a] structure solved or confirmed by SCXRD; [b] three heating/cooling cycles up to 1450°C

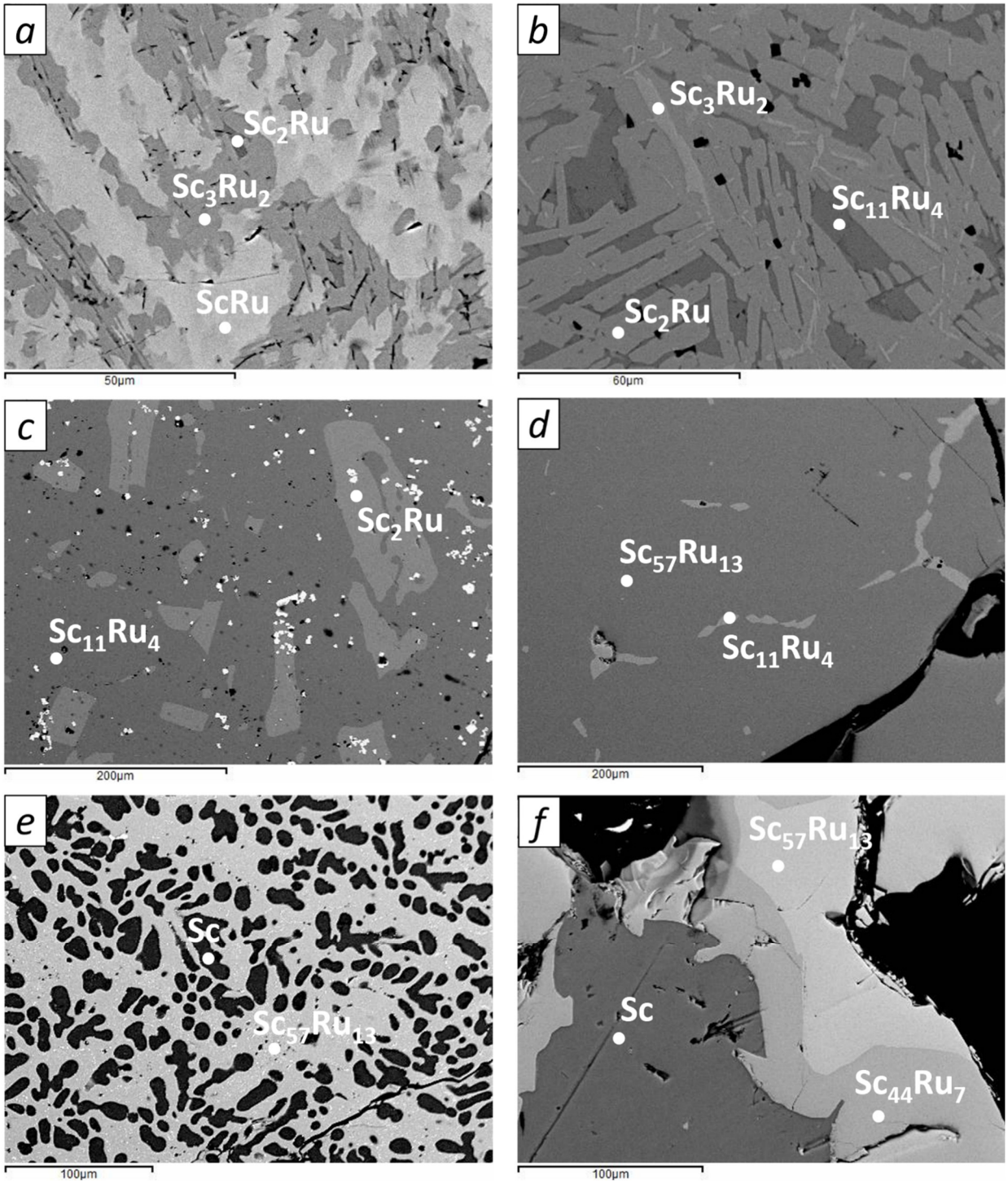


Fig. 5 SEM microphotographs (BSE mode) of selected Sc–Ru key alloys: a) N. 1 annealed; b) N. 4 as cast; c) N. 4 annealed (white crystals are Ta-containing impurities); d) N. 5 annealed; e) N. 6 as cast; f) N. 6 after three DTA cycles.

The 90 at.% Sc alloy showed an unusual behavior: in the as-cast state, it contained $Sc_{57}Ru_{13}$ and Sc, in agreement with the DC, but, after three heating/cooling cycles beyond the melting point, a non-equilibrium sample was obtained, where indeed $Sc_{44}Ru_7$ appeared. A reasonable explanation for the observations is that the formation temperature of $Sc_{44}Ru_7$ is lower than reported, probably below 850°C (it was not found in the DC at this temperature); on the other hand, the microstructure of the alloy (Fig. 5f) agrees with the peritectoid formation suggested in the literature. This idea is also in line with the convex hull [2,4].

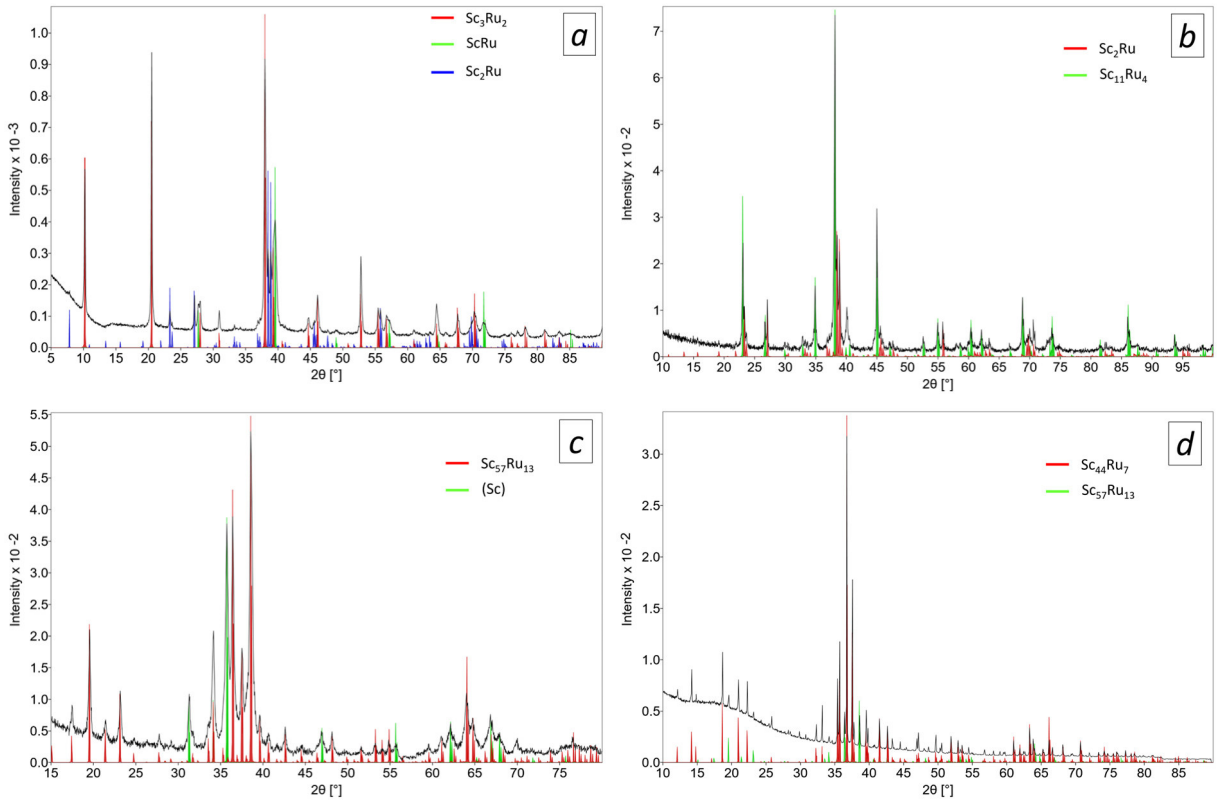


Fig. 6 Experimental (black lines) and calculated (colored lines) powder X-ray diffraction patterns of the Sc–Ru key alloys: a) N. 1 (59.1 at.% Sc, annealed); b) N. 4 (68.0 at.% Sc, annealed); c) N. 6 (89.6 at.% Sc, as cast); d) N. 6 (89.6 at.% Sc, after thermal cycles).

Table 2 Crystal data and single-crystal refinements for the Sc–Ru compounds confirmed in this work.

	$ScRu_2$	**ScRu**	**Sc_2Ru**	**$Sc_{11}Ru_4$**	**$Sc_{57}Ru_{13}$**	**$Sc_{44}Ru_7$**
Space group	*P*6$_3$/*mmc*	*Pm*-3*m*	*P*-3*m*	*Fm*-3*m*	*Pm*-3	*F*-43*m*
Pearson symbol, *Z*	*hP*12, 4	*cP*2, 1	*hP*45, 15	*cF*120, 8	*cP*140, 2	*cF*408, 8
Prototype	$MgZn_2$	CsCl	Sc_2Ru	$Sc_{11}Ir_4$	$Sc_{57}Rh_{13}$	$Mg_{44}Rh_7$
a [Å]	5.1242(3)	3.211(1)	9.3771(3)	13.3643(7)	14.4133(3)	20.7843(6)
c [Å]	8.5566(6)	–	11.3074(3)	–	14.4133(3)	–
Reflections collected	122	20	846	214	1344	1176
R_1 [$I \geq 2\sigma(I)$]	5.11	2.28	1.93	5.34	2.22	4.34
wR_2 [$I \geq 2\sigma(I)$]	5.98	2.36	2.93	5.14	3.97	5.48
R_1 [all data]	5.63	2.51	2.34	7.37	2.36	4.72
wR_2 [all data]	6.08	2.38	3.03	5.49	4.01	5.53
S [%]	3.59	1.29	1.73	2.60	2.64	2.79
$\Delta\rho$ [e/Å^3]	−2.29/2.40	−1.06/0.66	−1.08/0.67	−2.41/3.21	−0.47/0.73	−2.08/2.51

The crystal structures of the Sc–Ru compounds were studied both by single-crystal and powder X-ray diffraction. The single-crystal analyses of ScRu, Sc_2Ru, $Sc_{11}Ru_4$, $Sc_{57}Ru_{13}$, and $Sc_{44}Ru_7$ confirmed the previously reported structures: essential structural and refinement parameters are collected in Table 2. The powder X-ray diffraction data are also in perfect agreement (see Fig. 6).

For Sc_2Ru, the recently reported structure (*hP*45, own prototype) was confirmed in the studied temperature range. Based on these results, the previously reported *cF*96-Ti_2Ni structure [6] can be excluded; the *tI*6-Mo_2Si polymorph, proposed by Curtarolo *et al.* [2] by the convex hull construction, could be stable at low temperatures.

The compound Sc_3Ru_2 was found for the first time in this work: its diffraction pattern shows body-centered tetragonal symmetry with no additional systematic extinctions. A structural model was found using the intrinsic phasing method in the space group *I*4/*mmm* (N. 139). The unit cell contains 10 atoms, distributed over 2 sites for Sc and 1 for Ru. The possibility of a statistical mixture/partial occupation scenario was checked for each site, giving no improvements. The final anisotropic full-matrix least-squares refinements of the stoichiometric model converged to good residuals (see Table 3). The corresponding composition is in good agreement with EDXS measurements on several samples. In the refined structure all the interatomic distances are in line with the atomic sizes of the constituents.

Sc_3Ru_2 belongs to the Al_3Os_2 prototype with only six representatives known up to date [17]. Among the ternary compounds with ordered structures the chemically affine Er_2RuMg_2 can be mentioned [18]. The crystal structure is quite simple, representing one of the numerous variants of *bcc*-derived superstructures. Ordering with respect to the *cI*2-W aristotype can be represented in terms of a symmetry reduction in two steps: a translationengleiche (t3) one leading to the space group *I*4/*mmm* (*tI*2-In model) and an isomorphic (i5) one, retaining the tetragonal symmetry accompanied by splitting into three sites. These transformations are schematized in the form of a Bärnighausen tree [19,20] in Fig. 7, where the unit cell and coordination polyhedra of Sc_3Ru_2 are also shown. As a consequence of the shifts of atoms of different kinds, the coordination polyhedra of Ru1 and Sc2 have 13 vertices, one less than the classical rhombododecahedron, which is only maintained for Sc1.

Conclusions

The Sc–Ru phase equilibria were revised by combining studies of diffusion couples at 850 and 1000°C and of selected key alloys. The two approaches yielded consistent results, partially infirming previous literature:

- No evidence was found for Sc_5Ru_3, in agreement with the AFLOW data.
- The *hP*45-Sc_2Ru structure was confirmed, in line with energy cost criteria.
- $Sc_{44}Ru_7$ was observed after repeated thermal cycling of a Sc-rich alloy, but was absent in the diffusion couples: this suggests that its formation temperature is lower than previously reported.

Table 1 Crystal data and structure refinement for a Sc_3Ru_2 single crystal.

CCDC number	2583792
Empirical formula	Sc_3Ru_2
Pearson symbol-Prototype, *Z*	*tI*10-Al_3Os_2, 2
Space group	*I*4/*mmm* (139)
a [Å]	3.2432(3)
b [Å]	3.2432(3)
c [Å]	17.337(3)
Volume [Å^3]	182.36(4)
ρ_{calc} [g cm^{-3}]	6.138
μ [mm^{-1}]	13.117
Crystal size [mm^3]	0.02×0.05×0.08
Crystal color/shape	metallic silvery/irregular
Index ranges	$-5 \le h \le 4$; $-5 \le k \le 4$; $-26 \le l \le 28$
Reflections collected	811
Independent reflections	167; R_{int} = 0.037; R_{sigma} = 0.0338
Completeness to θ = 25.242°	98.6
Data / Restraints / Parameters	167 / 0 / 10
Goodness-of-fit on F^2	1.102
Final *R* indexes [$I \ge 2\sigma(I)$]	R_1 = 0.0483 wR_2 = 0.1194
Final *R* indexes [all data]	R_1 = 0.0632 wR_2 = 0.1287
$\Delta\rho$ [e/Å^3]	−1.73/6.99

atomic coordinates and equivalent displacement parameters

Atom	Wyckoff position	*x/a*	*y/b*	*z/c*	U_{eq}[a] [Å^2]
Ru1	4*e*	0	0	0.40457(8)	0.0112(4)
Sc1	2*a*	0	0	0	0.0113(13)
Sc2	4*e*	0	0	0.17750(2)	0.0132(6)

[a] U_{eq} is defined as 1/3 of the trace of the orthogonalized U_{ij} tensor

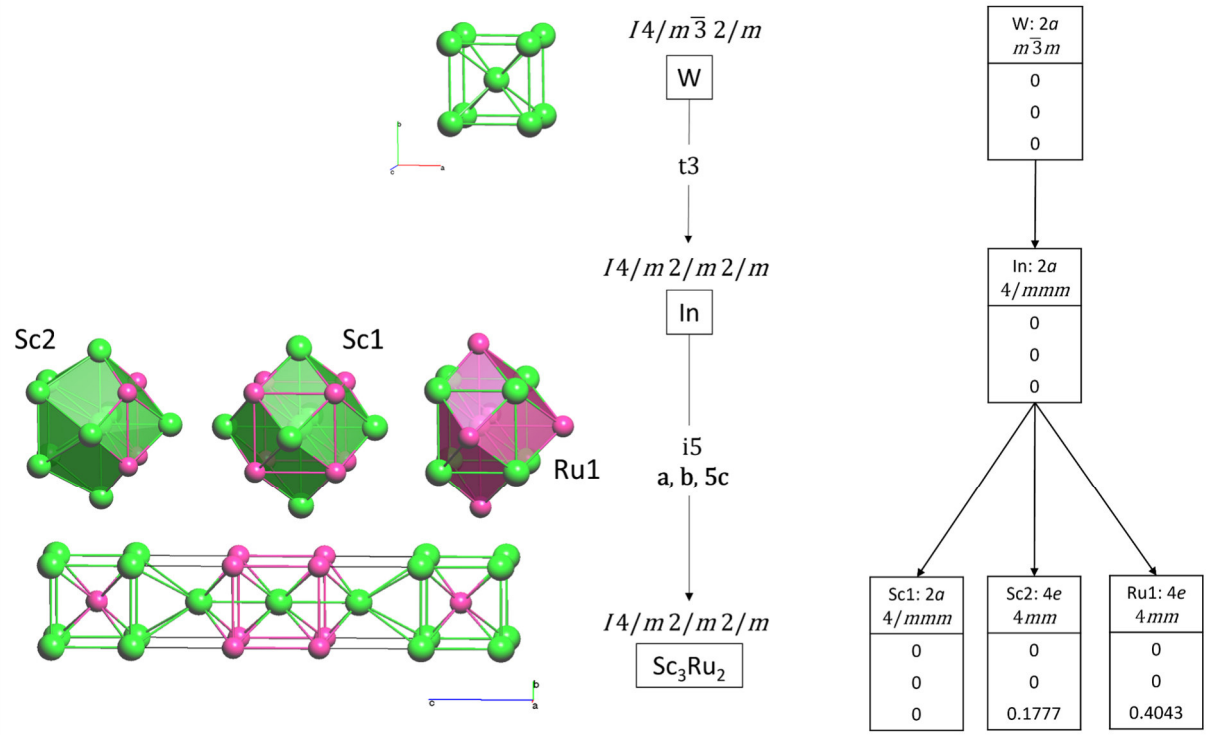


Fig. 7 Group-subgroup scheme in the Bärnighausen formalism for the structures of W, In and Sc_3Ru_2. The indices for the translationengleiche (t) and the isomorphic (i) symmetry reductions and the evolution of the atomic parameters are indicated. The coordination polyhedra and unit-cell content of Sc_3Ru_2 are shown on the left.

The new intermediate compound Sc_3Ru_2 was identified, representing the first 3:2 compound ever found in Sc–*T* systems. By single-crystal X-ray diffraction it was established that it crystallizes in the tetragonal Al_3Os_2 structure type (*I*4/*mmm*, *tI*10), representing a *bcc*-derived ordered superstructure. This structural model was not considered for the convex hull, which needs to be reassessed. Its discovery shows that the central compositional region of the Sc–Ru system is still uncertain.

More broadly, this study highlights diffusion couples as a rapid and resource-efficient tool for phase-diagram assessment, particularly when used together with targeted conventional synthesis to test and refine computational predictions. The recent developments in the field of electron crystallography open up new possibilities to conduct structural studies directly on nanocrystals extracted from interdiffusion layers. Our future studies will move in this direction.

Acknowledgements

Part of this work was done during Pietro Cattaneo's Master thesis project, carried out both at the University of Genova (Italy) and the University of Lund (Sweden) within the framework of the Erasmus+ program 'Outgoing for Traineeship'. The authors thank Pietro, as well as Prof. Sven Lidin, who supervised the work and provided materials and instruments at Lund University.

References

[1] S. Curtarolo, W. Setyawan, S. Wang, J. Xue, K. Yang, R.H. Taylor, L.J. Nelson, G.L.W. Hart, S. Sanvito, M. Buongiorno-Nardelli, N. Mingo, O. Levy, *Comput. Mater. Sci.* 58 (2012) 227-235. https://doi.org/10.1016/j.commatsci.2012.02.002

[2] G.L.W. Hart, S. Curtarolo, T.B. Massalski, O. Levy, *Phys. Rev. X* 3(4) (2013) 041035. https://doi.org/10.1103/PhysRevX.3.041035

[3] R. Freccero, P. Solokha, S. De Negri, *Inorg. Chem.* 60(14) (2021) 10084-10088. https://doi.org/10.1021/ACS.INORGCHEM.1C01168

[4] *http://www.aflowlib.org/*

[5] H. Okamoto, *J. Phase Equilib. Diffus.* 29(4) (2008) 387-388. https://doi.org/10.1007/S11669-008-9343-7

[6] V.N. Eremenko, V.G. Khorujaya, P.S. Martsenyuk, K.Y. Korniyenko, *J. Alloys Compd.* 217(2) (1995) 213-217. https://doi.org/10.1016/0925-8388(94)01321-7

[7] A.A. Kodentsov, G.F. Bastin, F.J.J. Van Loo, in: J.C. Zhao (Ed.), *Methods for Phase Diagram Determination,* Elsevier Science, 2007, pp. 222-245. https://doi.org/10.1016/B978-008044629-5/50006-9
[8] CrysAlis PRO. Agilent Technologies Ltd: Yarnton, Oxfordshire, England 2018.
[9] V. Petříček, M. Dušek, L. Palatinus, *Z. Kristallogr. - Cryst. Mater.* 229(5) (2014) 345-352. https://doi.org/10.1515/zkri-2014-1737
[10] APEX6. Bruker AXS Inc.: Madison, Wisconsin, USA 2026.
[11] SADABS. Bruker AXS Inc.: Madison, Wisconsin, USA 2016.
[12] G.M. Sheldrick, *Acta Crystallogr., Sect. C:Struct. Chem.* 71 (2015) 3-8. https://doi.org/10.1107/S2053229614024218
[13] G.M. Sheldrick, *Acta Crystallogr., Sect. A:Found. Adv.* 71 (2015) 3-8. https://doi.org/10.1107/S2053273314026370
[14] C.R. Groom, I.J. Bruno, M.P. Lightfoot, S.C. Ward, Acta Crystallogr., Sect. B:Struct. Sci., Cryst. Eng. Mater. 72 (2016) 171-179. https://doi.org/10.1107/S2052520616003954
[15] Kraus, W.; Nolze, G. POWDER CELL – a Program for the Representation and Manipulation of Crystal Structures and Calculation of the Resulting X-Ray Powder Patterns. *J. Appl. Crystallogr.* 29 (1996) 301-303.
[16] CrystalDiffract: A Powder Diffraction Program for Mac and Windows. CrystalMaker Software Ltd.: Oxford, England.
[17] P. Villars, K. Cenzual (Eds.), *Pearson's Crystal Data: Crystal Structure Database for Inorganic Compounds*, Release 2021/2022. ASM International, Materials Park, Ohio, USA.
[18] M. Kersting, O. Niehaus, R.D. Hoffmann, R. Pöttgen, *Z. Kristallogr.* 288(12) (2013) 643-649. https://doi.org/10.1524/ZKRI.2013.1692
[19] U. Müller, *Symmetry Relationships between Crystal Structures*; Oxford University Press, 2013 https://doi.org/10.1093/acprof:oso/9780199669950.001.0001
[20] U. Müller, Relating Crystal Structures by Group-Subgroup Relations, in: *International Tables for Crystallography*, Vol. A1, Ch. 1.6 (2011) pp. 44-56. https://doi.org/10.1107/97809553602060000795

Authors and ORCID IDs:
Serena DE NEGRI: 0000-0002-5345-8694
Pavlo SOLOKHA: 0000-0002-5252-635X

The paper is distributed under the terms of the Creative Commons Attribution Non-Commercial 4.0 (CC BY-NC) international license.